Dalton Transactions

PAPER

View Article Online
View Journal | View Issue

Cite this: *Dalton Trans.*, 2019, **48**, 15597

Polyoxometalate-based high-spin cluster systems: a NMR relaxivity study up to 1.4 GHz/33 T†

Masooma Ibrahim, [a] Steffen Krämer,[b] Nicolas Schork[c] and Gisela Guthausen *[c]

Paramagnetic polyoxometalates $[RE_{30}Co_8Ge_{12}W_{108}O_{408}(OH)_{42}(OH_2)_{30}]^{56-}$ (Rare Earth (RE): Gd, Dy, Eu, and Y) are of special interest with regard to their application as alternative contrast agents in non-human magnetic resonance imaging which is increasingly used in materials science and process engineering. This class of new paramagnetic materials promises detailed findings in the magnetic resonance images due to their rather large total electron spin on the one hand, *i.e.* large, field-dependent relaxivities up to the highest magnetic fields, and due to their relatively large cluster sizes with an impact on adsorption and penetration on the other hand. Apart from the magnetic field dependence, the sensitivity of relaxivities to motional correlation times will be shown for these polyoxometalates which is a prerequisite for modelling and understanding the physical behaviour of this new class of polyoxometalates in MRI. Also for the qualitative and quantitative interpretation of MR images, the knowledge of transverse and longitudinal relaxivities of the paramagnetic clusters in a given environment is mandatory. Examples considered in this publication are proteins in milk fractionation, the deposit of which was measured by MRI.

Received 16th May 2019,
Accepted 26th July 2019

DOI: 10.1039/c9dt02052g

rsc.li/dalton

Introduction

Polyoxometalates (POMs) constitute a structurally diverse class of discrete, negatively charged early transition metal oxide clusters. Their interesting structural, catalytic and magnetic properties can be explored in diverse fields such as catalysis, magnetism, or materials science.[1] Insertion of 3d- and 4f-transition metals into the lacunary derivatives of POMs led to functional inorganic materials.[2] Since POM ligands can be viewed as inorganic analogues of porphyrins, paramagnetic metal ions containing polyoxometalates (PM-POMs) could be designed and investigated as promising contrast agents.[3–7] A series of magnetic clusters, such as $[GdW_{10}O_{36}]^{9-}$, $[Gd(PW_{11}O_{39})_2]^{11-}$, $[Gd(BW_{11}O_{39})_2]^{15-}$, and $[Gd(CuW_{11}O_{39})_2]^{17-}$, have been synthesized and reported to exhibit higher r_1 than the commercial contrast agents.[4,8] This makes POMs promising prototypes for the development of new inorganic contrast agents which would be low-cost and easily tuneable to incorporate the paramagnetic centers. Studies have shown the ability of POMs to interact with amino acids: due to the negatively charged surface, POMs can strongly adhere to positively charged biological molecules, which exert an effect on the biocompatibility of PM-POMs as contrast agents.[9] The biocompatibility can be improved by constructing organic–POM hybrid assemblies by a combination of the polyanion with cationic organic molecules *via* noncovalent interactions.[10,11]

Recently, $[Dy_{30}Co_8Ge_{12}W_{108}O_{408}(OH)_{42}(OH_2)_{30}]^{56-}$, with the short name $\{Dy_{30}Co_8\}$,[10] a nano-sized heterometallic PM-POM, has been reported (Fig. 1),[12] which shows single-molecule magnet (SMM) behaviour. Other structural analogues $\{Gd_{30}Co_8\}$, $\{Eu_{30}Co_8\}$ and $\{Y_{30}Co_8\}$ were also synthesized following a similar synthetic procedure and were subsequently characterized by Fourier-transform infrared spectroscopy (FT-IR), elemental analysis, and thermogravimetric analysis. Furthermore, UV-VIS absorption spectra were used to prove the stability of these POMs in solution (see the ESI†).

$\{Dy_{30}Co_8\}$ and $\{Gd_{30}Co_8\}$ are extremely interesting ultra-high spin clusters because of not only their large range of the total electron spin (maximum for Dy: 237 and minimum for Y: 12), but also their topology and the directly related expectation of a high paramagnetic relaxation enhancement (PRE).

In order to generate a magnetic resonance image (MRI) contrast at rather small concentrations, contrast agents in MRI should typically not only provide a high PRE, but also exhibit dedicated penetration and adsorption properties. Last but not the least, from the application point of view, the relaxivities r_i ($i = 1, 2$) should ideally be independent of the MRI magnetic field currently commercially available up to 22.3 T (950 MHz ^{1}H frequency). r_i

[a]*Karlsruhe Institute of Technology (KIT), Institute of Nanotechnology (INT), Hermann-von-Helmholtz-Platz 1, D-76344 Eggenstein-Leopoldshafen, Germany*
[b]*Laboratoire National des Champs Magnétiques Intenses, LNCMI-CNRS (UPR3228), EMFL, Univ. Grenoble Alpes, INSA Toulouse, Univ. Toulouse Paul Sabatier, B.P. 166, 38042 Grenoble Cedex, France*
[c]*KIT, MVM-VM and EBI-WCT, Adenauerring 20b, D-76131 Karlsruhe, Germany. E-mail: gisela.guthausen@kit.edu*

†Electronic supplementary information (ESI) available. See DOI: 10.1039/c9dt02052g

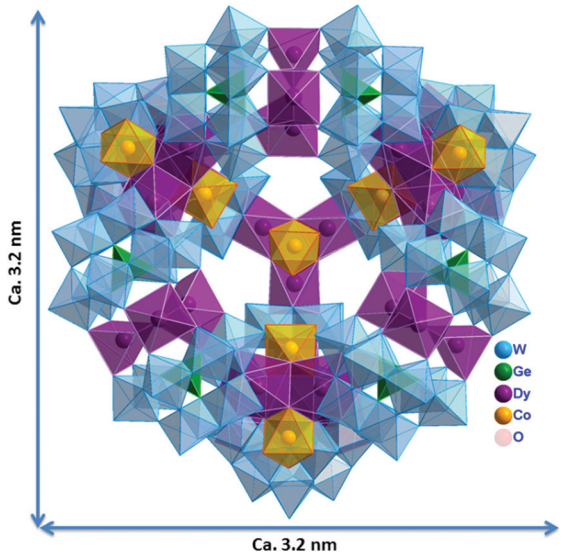

Fig. 1 $[Dy_{30}Co_8Ge_{12}W_{108}O_{408}(OH)_{42}(OH_2)_{30}]^{56-}$ in the polyhedral representation. Color code: WO_6 octahedra in blue, GeO_4 tetrahedra in green, CoO_6 in gold, and DyO_x in violet. The diameter of the POM is in the order of 3.2 nm.

should also be ideally independent of the direct molecular environment for facilitating an estimate of their concentration and the detection of eventual enrichment and penetration.

In this context, relaxivity studies provide some insight into the physical properties of $\{RE_{30}Co_8\}$ by varying the rare earth (RE) ions, and their impact on the total electron spin S_{total} and on the cooperative effects with the paramagnetic Co^{II} 3d ions can be explored. On the other hand, the magnetic field dependence of both longitudinal and transverse relaxivities up to the highest available magnetic fields provides insight into the physical mechanisms of PRE and the applicability as contrast agents, especially at the upcoming high fields in technical MRI in materials science and process engineering. The diverse theoretical contributions to PRE can be explored, which will allow a future in-depth description of the paramagnetism of the clusters. It is important to note that most of the particulate contrast agents often show negative charges, *i.e.* T_2 contrast, due to large transverse relaxivities,[13,14] but[15] the longitudinal relaxivity of commonly applied contrast agents usually decreases drastically with the magnetic field.[16,17] The contrast agents based on Gd show only a small field dependence, whereas the other lanthanides such as Dy have a pronounced field dependence with increasing r_i,[18–20] which is thought to be due to the much smaller electronic correlation times (Table 1).[16,17]

Apart from the application aspect of the clusters as contrast agents, the modelling and understanding of PRE is of importance when aiming at synthesizing an optimal compound in the sense of MRI contrast enhancement, adsorption, and local enrichment. To describe the different effects and contributions to PRE, a theoretical model considering the hyperfine interactions with the observed nuclei (usually ^1H of water molecules) and the dynamics in the form of correlation times was developed.[16,17] Often, inner and outer sphere contributions to PRE are discussed involving a variety of correlation times influencing the hyperfine interactions, which are responsible for PRE. These include diffusional, rotational and chemical exchange correlation times as well as electronic relaxation times. The variety of correlation times determining PRE needs to be sorted out in order to describe the physics of PRE of these POMs. The hyperfine interactions between the observed nuclei and the electron spins in the cluster are usually modelled by the isotropic Fermi contact and the anisotropic dipolar hyperfine interactions, exhibiting a strong distance dependence.

Results and discussion

The MR image contrast is most often given by the material's relaxation properties. In cases where the intrinsic relaxation differences are too small to reveal sufficient contrast of the structures searched for in MR images, contrast agents may be applied to magnify structural differences by PRE. But not only the contrast enhancement application should be mentioned. Dynamic processes including sorption, penetration, and accumulation of species can be detected and even quantified by exploring the possibilities of PRE.

As PRE must obviously depend on the concentration of the paramagnetic species, relaxivities r_i (i = 1,2) were introduced which represent the relaxation rates normalized to the concentration. These quantities represent the ability of a paramagnetic moiety to enhance the relaxation of neighbouring molecules, in most cases of water. They are used for comparative studies of contrast agents and a theoretical description of PRE. It is noteworthy that 30 RE ions contribute to the total electron spin of $\{RE_{30}Co_8\}$. Apart from Y^{III}, different lanthanide ions were studied with similar orbital overlap with the eight paramagnetic Co^{II} ions. 24 coordination sites are available for

Table 1 Some physical parameters of the relevant elements determining PRE in $\{RE_{30}Co_8\}$ POMs[17,19–21]

RE	Electron spin	Electronic correlation time [s]	Maximum total electron spin (ferromagnetic ordering assumed) S_{total}
Gd^{III} (4f)/POM	7/2	10^{-7}—10^{-10}	117 (including Co^{II})
Dy^{III} (4f)/POM	15/2	10^{-13}	237 (including Co^{II})
Eu^{III} (4f)/POM	0		12 (including Co^{II})
Y^{III} (3d)/POM	0		12 (including Co^{II})
Co^{II} (3d)/ion	3/2	10^{-11}–10^{-12}	12

water molecules, which determine the PRE. Additionally, the mentioned residence times, *i.e.* diffusional and rotational correlation times, as well as the chemical exchange are essential, of course.

Longitudinal relaxivity: field dependence for $\{RE_{30}Co_8\}$ (RE∈[Gd, Dy, Eu, Y])

PRE induces a positive image contrast *via* longitudinal relaxation as it reduces the longitudinal relaxation time and therefore enhances the signal intensity in T_1 weighted images. This effect should be at its maximum at the given magnetic field of the magnetic resonance instrumentation, which is nowadays commercially available up to 22.3 T, with a ^{1}H frequency of 950 MHz with 28 T/1200 MHz in perspective. It allows for a faster measurement, less T_1 saturation and therefore signal loss. The longitudinal relaxivities of $\{RE_{30}Co_8\}$ (Fig. 2) show a pronounced field dependence: the classic observation of a strong decrease around 100 MHz (ref. 16 and 22) is replaced by a pronounced increase for RE = Dy and a gradual decrease for RE = Gd, which indicates the necessity to apply the highest available magnetic fields in order to obtain the largest possible extent of field ranges for modelling of the underlying mechanisms. Similar behaviour was found for ultra-high spin clusters $Fe_{10}Ln_{10}$.[18,23] It is noteworthy that the number of POM clusters was chosen as the concentration unit rather than usually the number of ions. The motivation is that the cluster will act as a whole rather than as individual, independent ions. As the effects of 4f *vs.* 3d orbital configurations and of RE and Co ions on PRE were of interest, the present representation seems adequate even though unusual.

A differentiation of the contributions of RE ions and Co ions to PRE was achieved by the variation of RE (Table 1): Eu^{III} is diamagnetic, but still a 4f element: the corresponding POM shows a small PRE due to the few leftover paramagnetic Co^{II} ions. Its PRE changes with the replacement of Eu^{III} by the diamagnetic rare earth metal Y^{III} ion, leading to a decrease in r_1, especially at the highest magnetic fields, *i.e.* ^{1}H Larmor frequencies ν. This observation is a strong hint of significant orbital overlap and correlative effects between the 4f and 3d orbitals in these POMs (Fig. 3).

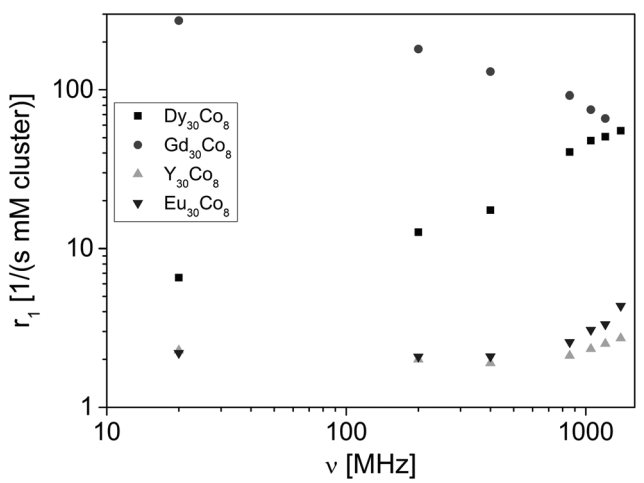

Fig. 2 Longitudinal relaxivities r_1 of $\{RE_{30}Co_8\}$ POMs in water. The field dependence of r_1 is mainly due to the electronic relaxation times. The differences in PRE for different RE in r_1 is due to the total electron spin and the electronic correlation times, and also due to correlative effects (compare 3d Y^{III} with 4f Eu^{III}).

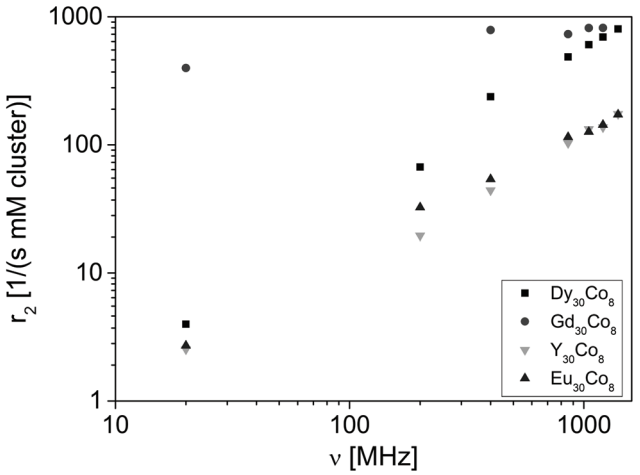

Fig. 3 Transverse relaxivities r_2 of $\{RE_{30}Co_8\}$ in water. The different metal ions in the POM lead to different orders of magnitude and field-dependent transverse relaxivities; the logarithmic scale is to be noted.

As the magnetic fields of current MR instrumentation tend to increase even further also in medical diagnostics, it is interesting to note that the difference in r_1 between Gd and Dy containing POMs decreases with ν. This is especially relevant, as the Gd metal ion is known to be toxic, whereas the Dy metal ion is believed to be non-toxic.

Transverse relaxivity: field dependence for $\{RE_{30}Co_8\}$ (RE∈[Gd, Dy, Eu, Y])

The transverse relaxation determines the image contrast, as does the longitudinal relaxation. However, instead of providing a positive effect (increased signal intensity) due to the shorter longitudinal relaxation caused by PRE, a shorter PRE-induced transverse relaxation leads to a negative effect, *i.e.* a decrease of the signal intensity in the images. In addition, the transverse relaxivity shows a pronounced magnetic field dispersion. For all $\{RE_{30}Co_8\}$, r_2 increases. In this case, a parallelism with the electronic correlation time is evident. Interestingly, the exchange of Eu and Y metal ions leads to a less pronounced effect, indicating that the correlative effects are not as significant on the time scale of transverse relaxation. The value of r_2 at large ν compared to r_1 is also to be noted. Very small amounts of POMs will have a huge impact on the image contrast leading to an enormous sensitivity. The findings are in contrast to the observations on nanoparticles where the transverse relaxivities decrease with the field.

Clustering and effects of solvent on relaxivities

Molecular interactions as well as size and conformational stability play a major role with regard to the selectivity, pene-

tration and permeation of POMs into materials. Transport phenomena in porous media can be studied in detail – provided the relaxivities are known and significant. Agglomeration, clustering and aggregation of the paramagnetic moieties are known to reduce the longitudinal relaxivities, while the transverse relaxivities are known to be less affected. This behaviour is well known from (super-)paramagnetic iron oxide nano-crystallites indicating the dependence on the rotational correlation time. Therefore, a diameter of 3.2 nm of the $Ln_{30}Co_8W_{108}$ clusters seems to be a good choice for integrating a large total spin and appropriate diffusional, rotational and chemical exchange correlation times for a significant PRE.

PRE is usually explored for aqueous solutions of the PRE-inducing moieties. In an application as a contrast agent, this constellation is usually not given in the real environment – neither in medical diagnostics nor in technical applications, such as transport studies in biofilms or in filtration. The question has to be answered whether the chemical and physical properties of a solvent significantly influence PRE. The effect was already shown for a Mn-induced PRE.[24,25] It has major implications in image interpretation and even more in quantification. For example, the calculation of concentration maps is only possible when knowing the PRE in the corresponding environments. This issue was therefore also addressed for the PRE of $\{RE_{30}Co_8\}$. To allow a direct comparison of relaxivities, water relaxation should be measured while varying the solvent's composition. This can be achieved either by modifying the composition by adding deuterated solvents soluble in water or by exploring the spectral resolution when using conventional additional solvents. In a first attempt, 1,2-propanediol was added in various amounts with the aim of modifying the viscosity and therefore the diffusional and rotational correlation times of the solution (Fig. 4a). In a first example, PRE was explored for the ultra-high spin cluster $\{Fe_{10}Dy_{10}\}$ in a concentration of 1 mM. The longitudinal dispersion diminished drastically (Fig. 4b), and the transverse dispersion showed a maximum at an effective diffusion coefficient of about 4×10^{-10} m^2 s^{-1} (Fig. 4c). This first example shows that the rotational and diffusional degrees of freedom influence the paramagnetic relaxation enhancement drastically.

The cluster's shape of $\{RE_{30}Co_8\}$ differs from that of $\{Fe_{10}Dy_{10}\}$, with the possibility of exchanging water chemically, and in the accessibility of the paramagnetic centres by water molecules. Nevertheless, the question should be answered whether the relaxation behaviour depends as strongly on the chemical composition of the environment as in the case of $\{Fe_{10}Dy_{10}\}$. Thus, the relaxation dispersion was measured for Larmor frequencies between 20 MHz and 1.4 GHz. The solvent composition was changed implicating a variation of the $\{Gd_{30}Co_8\}$ concentration. If the solvent composition has no effect on the relaxation properties, the dependence on the concentration is linear. Interestingly, a field-dependent deviation from this expectation is observed (Fig. 5). This indicates that the environment, *i.e.* its chemical composition and molecular interaction, has to be considered in detail in the case in which

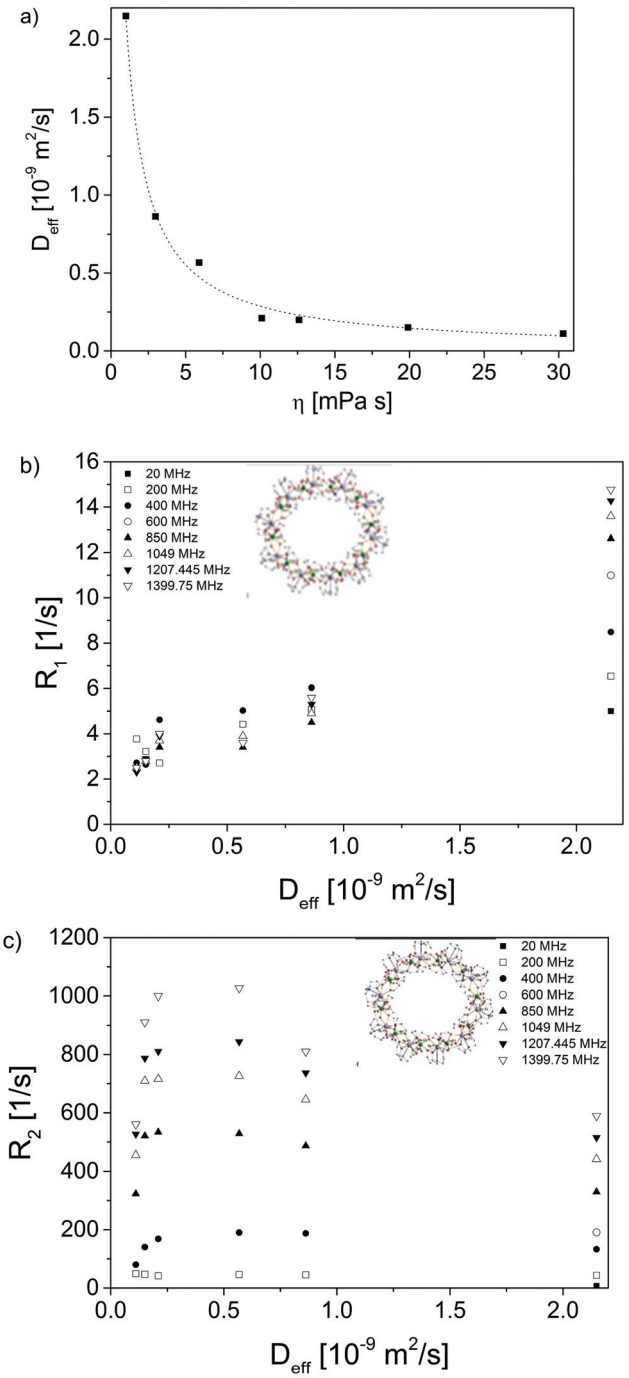

Fig. 4 (a) Water diffusion coefficient *versus* viscosity of a mixture of 1,2-propanediol and water. With increasing concentration of 1,2-propanediol, the viscosity increases while the water diffusion coefficient decreases. (b) Longitudinal relaxation dispersion and (c) transverse relaxation dispersion of the $\{Fe_{10}Dy_{10}\}$ ultra-high spin cluster as a function of the diffusion coefficient.

contrast agent concentrations are to be deduced from MR images. A comparably simple example in terms of interaction possibilities will be discussed below in the form of milk filtration.

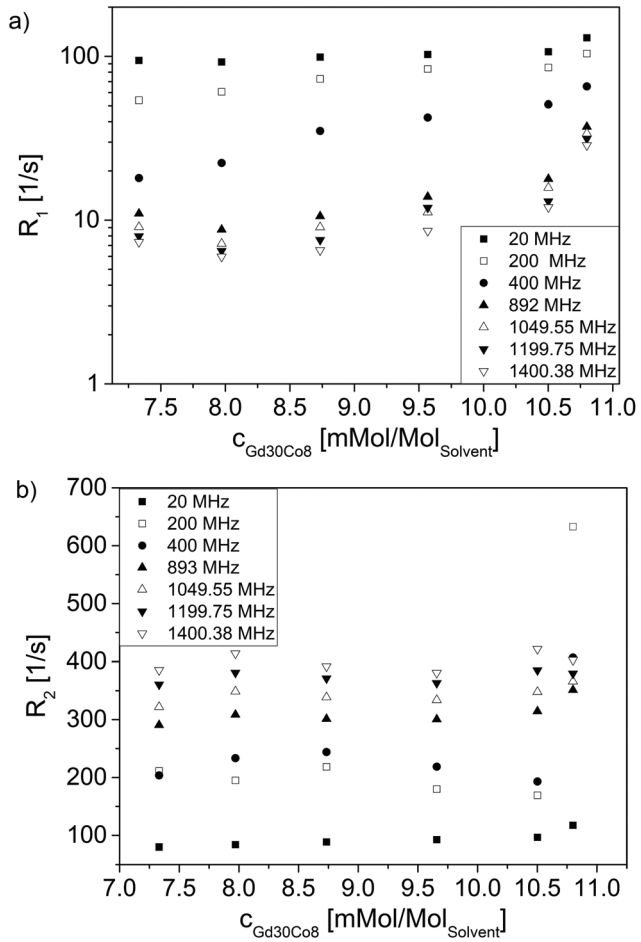

Fig. 5 (a) The longitudinal relaxation rate R_1 in water/1,2-propanediol mixtures does not show the expected linear dependence on the concentration; nevertheless, a relaxation dispersion is evident. Especially at low Larmor frequencies, a more or less constant relaxation rate was measured. (b) A similar behaviour was found for the corresponding transverse relaxation rate. In this case, the expected linear behaviour is also not observed – with a strong impact on a possible quantification of the contrast agent concentration.

Magnetic resonance imaging with $\{RE_{30}Co_8\}$: an example

MRI can be utilized to characterize technical processes and products. In order to enhance the image's contrast, contrast agents can be applied. Not only faster measurements are possible due to longitudinal PRE, especially when monitoring time-dependent processes, but also questions of penetration and adsorption of the contrast agent by various materials can be addressed. This was shown in the example of biofilms[18,26] for $\{Fe_{10}Ln_{10}\}$. In this paper, we use a filtration process to look into the adsorption and penetration properties of the PM-POMs.

$\{Gd_{30}Co_8\}$ was applied in an in–out membrane filtration process for the fractionation of skimmed milk proteins.[27] Questions of penetration and adsorption are essential as the average pore size of the ceramic hollow fiber membrane is in the order of 40 nm and the PM-POMs are 3.2 nm in diameter. In the case in which they penetrate the deposit layer, the clusters will also penetrate the membrane. A changed contrast in the MR images will therefore indicate a strong interaction of PM-POM with the diverse proteins in addition to the improved image contrast, which enables the quantification of the deposits. In skimmed milk filtration, the residues on the inside of the hollow fibre membrane consist primarily of casein proteins. This deposit leads to a decrease in the whey protein throughput and therefore a decrease of the overall product efficiency. Detailed knowledge of the formation and structural composition of the deposit layer is therefore preferable when addressing technical filtration improvements.

In previous studies,[28–30] particulate contrast agents were added to the skimmed milk feed solution to enhance the MRI contrast of the deposit *vs.* feed, which is a prerequisite for quantification of the images. Here, a milk protein deposit was accumulated on the membrane surface (Fig. 6a and b), before 100 µl of an aqueous solution of $\{Gd_{30}Co_8\}$ was in-line injected into the feed stream using a 6-way valve. Due to the continuous filtration, the clusters are filtered with the feed solution in the membrane, forming a second layer on top of the already existing protein deposit (Fig. 6c).

To quantify the deposit and the distribution of the skimmed milk proteins in the lumen of the hollow fibre membrane, dedicated image processing was applied. The signal intensity on the inside of the hollow fibre is radially averaged in rings one pixel wide. The mean signal intensity as a function of the radius then reflects the desired quantities. During dead-end filtration, proteins progressively accumulate at the

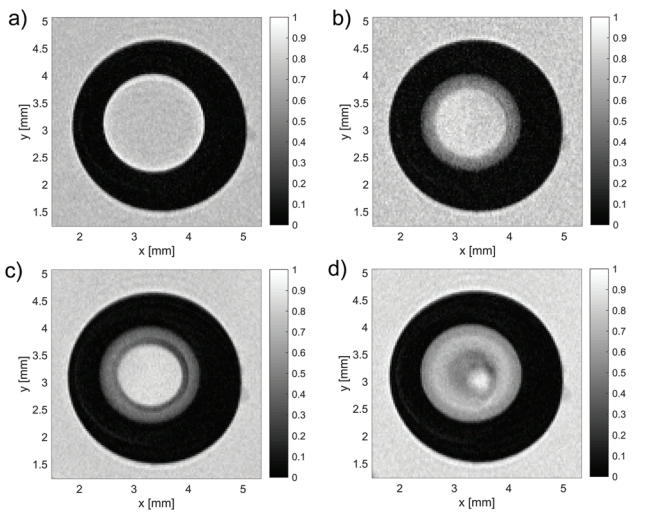

Fig. 6 Axial MR images during an *in situ* dead-end membrane filtration of skimmed milk with a feed pressure p = 1.5 bar. (a) Axial reference image of the ceramic hollow fibre membrane before starting the filtration. (b) After t = 3 h 10 min, a thick deposit layer was formed at the inside of the hollow fibre. (c) After applying the contrast agent, a second layer containing $\{Gd_{30}Co_8\}$ also forms with a lower signal intensity, *i.e.* $\{Gd_{30}Co_8\}$ enhances the image contrast (filtration time t = 4 h 40 min), but does not penetrate the deposit despite the pressure. (d) Back diffusion: the moieties in the second filtration layer containing the contrast agent diffuse back into the inner membrane lumen, while the first part of the deposit remained attached to the membrane surface.

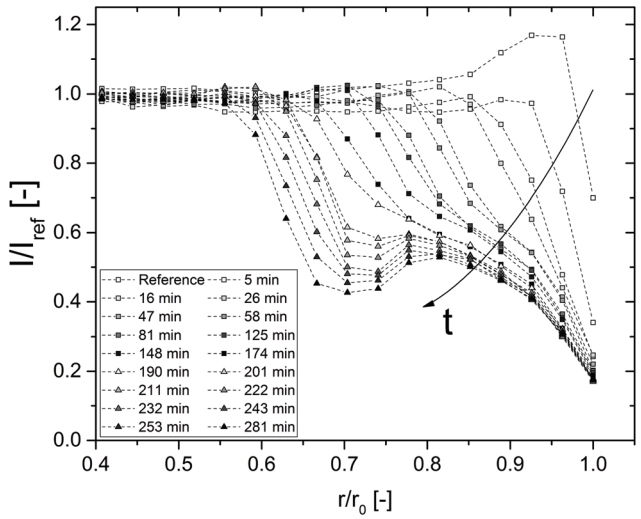

Fig. 7 Normalized intensity in the hollow fibre membrane as a function of the radius at diverse filtration times. After a filtration time of t = 190 min, the $\{Gd_{30}Co_8\}$ solution was injected, while the filtration continued. The second layer on top of the deposit was identified due to the reduced signal ($r/r_0 \in [0.65, 0.75]$). All lines are guides to the eye.

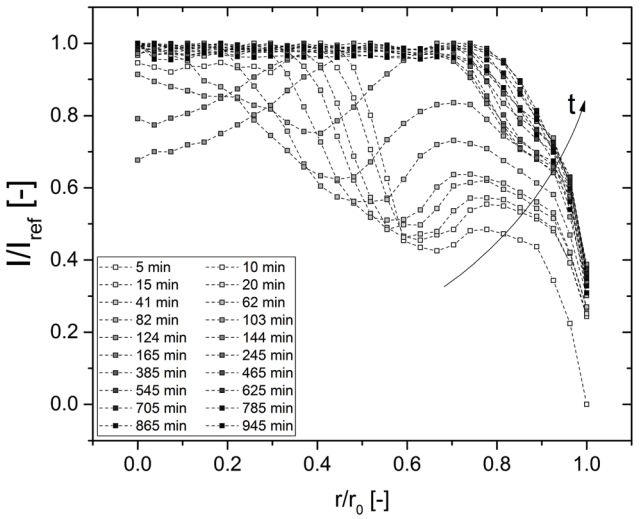

Fig. 8 Signal intensity distribution in the hollow fibre membrane as a function of time and radius in the back-diffusion experiment after the feed pressure was released. The built-up cluster-containing layer seems to diffuse independently from the first deposit layer. Even after t = 16 h, a small fraction of the deposit layer remains attached to the membrane. All lines are guides to the eye.

membrane surface, resulting in a lower signal intensity (I/I_{ref}) with progressing filtration time (Fig. 7).

The clusters in the skimmed milk solution, which are filtered towards the already existing deposit layer, are accumulated together with milk proteins. A second deposit layer builds up. Due to the faster relaxation of proteins and water molecules in the nearest neighbourhood of the clusters, the signal intensity is reduced compared to the intensity of the first deposit (Fig. 6c and 7, triangles). The first deposit layer of milk proteins appears to be dense enough or to interact strongly enough with the PM-POM to hardly allow a penetration of the clusters through the deposit layer as a decrease in the signal intensity was barely observed in the first deposit layer or in the permeate channel.

Subsequently, the feed pressure was released to observe a possible back diffusion as no convective forces towards the membrane surface were present. Back diffusion reveals the nature of the deposits, which is in the extremes, *i.e.* either a semisolid-like gel or a concentration gradient of loose moieties.

According to Fick's law, only the concentration gradient forces back diffusion. A concentration gradient would tend to be equilibrated. The clusters would diffuse back towards the inner membrane lumen, as do loosely bound proteins. In the experiment, signal intensities were found to decrease at smaller normalized radii with progressing time for back diffusion (Fig. 8). The second deposit layer seems to diffuse independently from the first layer of pure protein accumulation, which remains on the membrane surface even after a back-diffusion time of 16 h (Fig. 8 and 6d). The radial signal intensity distribution reflects the inhomogeneous back diffusion of the protein–cluster mixture in the feed channel.

Experimental

Synthetic procedures and topology of $\{RE_{30}Co_8\}$

$\{Dy_{30}Co_8\}$ was synthesized in simple one-pot reactions of $CoCl_2{\cdot}6H_2O$ and $Dy(NO_3)_3{\cdot}5H_2O$ with $Na_{10}[A\text{-}\alpha\text{-}GeW_9O_{34}]{\cdot}18H_2O$ in aqueous medium at pH 8 in the presence of LiOH, and then isolated as a hydrated salt, $Cs_{14}Co_6Na_{30}[RE_{30}Co_8Ge_{12}W_{108}O_{408}\ (OH)_{42}(OH_2)_{30}]_{ca.\ 370}$, with the short name $\{Dy_{30}Co_8\}$. Single crystal X-ray diffraction analysis revealed that the poly-anion $\{Dy_{30}Co_8\}$ is a tetrahedral nano-cage which results from the assembly of two types of subunits including four $\{Co^{II}_2Dy^{III}_3(\mu_3\text{-}OH)_6(OH_2)_6\}$ hetero-metallic entities (nodes) which define the tetrahedron corners and six $\{(GeW_9O_{34})_2Dy^{III}_3(\mu\text{-}OH)_3(H_2O)\}$ homo-metallic motifs (linkers) which are placed along the tetrahedron edges. The hollow tetrahedron has a side length of *ca.* 3.2 nm and is filled by a number of water molecules and counter cations. The synthetic conditions of other isostructural poly-anions $\{RE_{30}Co_8\}$ (RE = Gd, Eu, Y) are identical (ESI†).

NMR relaxation dispersion measurements

In the relaxivity study, several NMR systems were used in order to cover the interesting Larmor frequency range from 20 MHz to 1.4 GHz. Relaxation times were measured at diverse Larmor frequencies ν, involving diverse MR instrumentation. "Bruker the minispec" mq20 was used for T_1 and T_2 relaxation at ν = 20 MHz. T_1 was measured using a progressive saturation recovery pulse sequence and T_2 using a CPMG multi-echo sequence. At 200 MHz, a Bruker MRI machine was used, and at 400 MHz, a Bruker WB spectrometer with corresponding Topspin software for data acquisition. Data could be described by mono-exponential functions to the level of experimental noise. This

Table 2 RARE pulse sequence parameters for *in situ* MR measurements of dead-end filtration and back diffusion

RARE parameters	Value
T_R	4 s
τ_E	5.5 ms
RF	2
Number of averages	1 (4)
Pixel size $\Delta x = \Delta y$	32.5 μm
Slice thickness Δz	3 mm
Scan time	5 min 8 s (20 min 32 s)
Encoding order	Centric
Partial Fourier factor (phase)	1.3

model was therefore applied to deduce relaxation times, *i.e.* the corresponding relaxation rates from the raw data. All samples were measured at room temperature.

At the Laboratoire National des Champs Magnétiques Intenses (LNCMI) in Grenoble, a 24 MW resistive magnet provides variable fields up to 37 T in a 34 mm room temperature bore which were used up to 33 T/1.4 GHz in this study. Details of the measurements are reported in the studies in ref. 18 and 23.

Relaxivities are determined *via* measuring relaxation rates as a function of the POM concentration. The expected linear behaviour was found in aqueous solutions. The relaxivities were therefore determined as the slope in a linear regression.

MRI for skim milk filtration

A "Rapid Acquisition with Relaxation Enhancement" (RARE) MRI pulse sequence was chosen to allow fast data acquisition during the time-dependent filtration experiments. The time resolution was about 5 min per image and about 20 min for the averaging during the back-diffusion measurements *via* four scans. In order to avoid flow artifacts, the repetition time (T_R) needs to be set sufficiently long, and the RARE factor (RF) was chosen to be rather low. The main parameters are summarized in Table 2.

Conclusions

The NMR relaxivity measurements of $\{RE_{30}Co_8\}$ exhibited highly improved relaxation ability in comparison with those of Gd-based commercially available contrast agents. Presently, we focus on the development of high-spin clusters within a polyoxometalate (POM) framework in order to systematically expand our quest for more efficient contrast agents. In other words, a large variety of paramagnetic metal-containing polyoxometalates will enable us to further study the efficiency of the paramagnetic metal in shortening T_1 and T_2. In addition to relaxivities, adsorption and penetration behaviour will be investigated.

Conflicts of interest

There are no conflicts to declare.

Acknowledgements

M. I. thanks the German Science Foundation (DFG-IB 123/1-1) and the Institute of Nanotechnology (INT) at the Karlsruhe Institute of Technology for research support. Amer Baniodeh and Yvonne Maier contributed to the synthesis and relaxation measurements of the $Fe_{10}Ln_{10}$ clusters. Audrey Zoulim developed a part of the data analysis software used for the experiments at LNCMI. Prof. Dr Annie Powell is greatly acknowledged for her work. The financial support of DFG is highly acknowledged (Pro^{2}NMR @ KIT), as well as the financial support in the IGF Project of the FEI which is supported *via* AiF within the programme for promoting the Industrial Collective Research (IGF) of the German Ministry of Economic Affairs and Energy (BMWi), based on a resolution of the German Parliament.

Notes and references

1 D.-L. Long, R. Tsunashima and L. Cronin, *Angew. Chem., Int. Ed.*, 2010, **49**, 1736–1758.
2 S. Reinoso, *Dalton Trans.*, 2011, **40**, 6610–6615.
3 J. Feng, G. Sun, F. Pei and M. Liu, *J. Inorg. Biochem.*, 2002, **92**, 193–199.
4 J. Feng, X. Li, F. Pei, G. Sun, X. Zhang and M. Liu, *Magn. Reson. Imaging*, 2002, **20**, 407–412.
5 B. S. Bassil, M. Ibrahim, R. Al-Oweini, M. Asano, Z. Wang, J. van Tol, N. S. Dalal, K.-Y. Choi, R. Ngo Biboum, B. Keita, L. Nadjo and U. Kortz, *Angew. Chem., Int. Ed.*, 2011, **50**, 5961–5964.
6 M. Ibrahim, A. Haider, Y. Lan, B. S. Bassil, A. M. Carey, R. Liu, G. Zhang, B. Keita, W. Li, G. E. Kostakis, A. K. Powell and U. Kortz, *Inorg. Chem.*, 2014, **53**, 5179–5188.
7 M. Ibrahim, Y. Lan, B. S. Bassil, Y. Xiang, A. Suchopar, A. K. Powell and U. Kortz, *Angew. Chem., Int. Ed.*, 2011, **50**, 4708–4711.
8 Z. Li, W. Li, X. Li, F. Pei, Y. Li and H. Lei, *Magn. Reson. Imaging*, 2007, **25**, 412–417.
9 L. Zheng, Y. Ma, G. Zhang, J. Yao, B. S. Bassil, U. Kortz, B. Keita, P. de Oliveira, L. Nadjo, C. T. Craescu and S. Miron, *Eur. J. Inorg. Chem.*, 2009, **2009**, 5189–5193.
10 H. Li, H. Sun, W. Qi, M. Xu and L. Wu, *Angew. Chem., Int. Ed.*, 2007, **46**, 1300–1303.
11 W. Chai, S. Wang, H. Zhao, G. Liu, K. Fischer, H. Li, L. Wu and M. Schmidt, *Chem. – Eur. J.*, 2013, **19**, 13317–13321.
12 M. Ibrahim, V. Mereacre, N. Leblanc, W. Wernsdorfer, C. E. Anson and A. K. Powell, *Angew. Chem., Int. Ed.*, 2015, **54**, 15574–15578.
13 Q. L. Vuong, S. Van Doorslaer, J. L. Bridot, C. Argante, G. Alejandro, R. Hermann, S. Disch, C. Mattea, S. Stapf and Y. Gossuin, *Magn. Reson. Mater. Phys., Biol. Med.*, 2012, **25**, 467–478.
14 Q. L. Vuong, J. F. Berret, J. Fresnais, Y. Gossuin and O. Sandre, *Adv. Healthcare Mater.*, 2012, **1**, 502–512.

15 Y. Gossuin, A. Hocq, Q. L. Vuong, S. Disch, R. P. Hermann and P. Gillis, *Nanotechnology*, 2008, **19**(47), 475102.
16 I. Bertini, C. Luchinat and G. Parigi, *Solution NMR of paramagnetic molecules: Applications to metallobiomolecules and models*, Elsevier Science B.V., Amsterdam, 1st edn, 2001.
17 I. Bertini, C. Luchinat, G. Parigi and E. Ravera, *NMR of Paramagnetic Molecules - Applications to Metallobiomolecules and Models*, Elsevier, Amsterdam, 2017.
18 G. Guthausen, J. R. Machado, B. Luy, A. Baniodeh, A. K. Powell, S. Krämer, F. Ranzinger, M. P. Herrling, S. Lackner and H. Horn, *Dalton Trans.*, 2015, **44**, 5032–5040.
19 E. Debroye, S. Laurent, L. Vander Elst, R. N. Muller and T. N. Parac-Vogt, *Chem. – Eur. J.*, 2013, **19**, 16019–16028.
20 L. Vander Elst, A. Roch, P. Gillis, S. Laurent, F. Botteman, J. W. M. Bulte and R. N. Muller, *Magn. Reson. Med.*, 2002, **47**, 1121–1130.
21 G. Pintacuda, M. John, X. C. Su and G. Otting, *Acc. Chem. Res.*, 2007, **40**, 206–212.
22 S. Aime, M. Botta and E. Terreno, in *Advances in Inorganic Chemistry*, Academic Press, 2005, vol. 57, pp. 173–237.
23 J. R. Machado, A. Baniodeh, A. K. Powell, B. Luy, S. Krämer and G. Guthausen, *ChemPhysChem*, 2014, **15**, 3608–3613.
24 I. Bertini, F. Briganti, Z. C. Xia and C. Luchinat, *J. Magn. Reson., Ser. A*, 1993, **101**, 198–201.
25 I. Bertini, F. Capozzi, C. Luchinat, G. Nicastro and Z. C. Xia, *J. Phys. Chem.*, 1993, **97**, 6351–6354.
26 F. Ranzinger, M. P. Herrling, S. Lackner, V. W. Grande, A. Baniodeh, A. K. Powell, H. Horn and G. Guthausen, *Acta Biomater.*, 2016, **31**, 167–177.
27 N. Schork, S. Schuhmann, H. Nirschl and G. Guthausen, *Magn. Reson. Chem.*, 2019, 1–11, DOI: 10.1002/mrc.4826.
28 S. Schuhmann, N. Schork, K. Beller, H. Nirschl, T. Oerther and G. Guthausen, *AIChE J.*, 2018, **64**, 4039–4046.
29 N. Schork, S. Schuhmann, F. Arndt, S. Schütz, G. Guthausen and H. Nirschl, *Microporous Mesoporous Mater.*, 2018, **269**, 60–64.
30 F. Arndt, S. Schuhmann, G. Guthausen, S. Schütz and H. Nirschl, *J. Membr. Sci.*, 2017, **524**, 691–699.